Proceedings of the ASME 2014 International Design Engineering Technical Conferences & Computers and Information in Engineering Conference
IDETC/CIE 2014
August 17-20, 2014, New York, United States

DETC2014-34897

OPTIMAL DUAL-MODE HYBRID ELECTRIC VEHICLE POWERTRAIN ARCHITECTURE DESIGN FOR A VARIETY OF LOADING SCENARIOS

Alparslan Emrah Bayrak *
Mechanical Engineering
University of Michigan
Ann Arbor, Michigan, 48109
Email: bayrak@umich.edu

Yi Ren
Mechanical Engineering
University of Michigan
Ann Arbor, Michigan, 48109
Email: yiren@umich.edu

Panos Y. Papalambros
Mechanical Engineering
University of Michigan
Ann Arbor, Michigan, 48109
Email: pyp@umich.edu

ABSTRACT

A hybrid-electric vehicle powertrain architecture consists of single or multiple driving modes, i.e., connection arrangements among engine, motors and vehicle output shaft that determine distribution of power. While most architecture development work to date has focused primarily on passenger cars, interest has been growing in exploring architectures for special-purpose vehicles such as vans or trucks for civilian and military applications, whose weights or payloads can vary significantly during operations. Previous findings show that the optimal architecture can be sensitive to vehicle weight. In this paper we investigate architecture design under a distribution of vehicle weights, using a simulation-based design optimization strategy with nested supervisory optimal control and accounting for powertrain complexity. Results show that an architecture under a single load has significant differences and lower fuel efficiency than an architecture designed to work under a variety of loading scenarios.

1 Introduction

A powertrain driving mode of a Hybrid-Electric Vehicle (HEV) is defined as the the connection arrangement among engine, Motor/Generators (MG) and vehicle output shafts. For example, the Toyota Prius powertrain has one driving mode represented by a lever analogy, as shown in Figure 1. Here the Planetary Gear (PG) is represented by the lever. It splits the power demand from the vehicle output shaft into the engine and MGs.

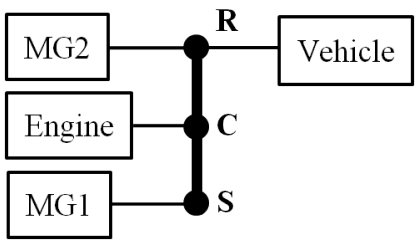

FIGURE 1. The Toyota Prius Hybrid System in the lever representation; four powertrain components (the engine, two MGs and the vehicle output shaft) are connected to PG nodes.

We refer to a powertrain architecture as a collection of driving modes. For instance, the Chevrolet Volt has a four-mode architecture, which uses clutches to switch among modes, in order to achieve high fuel efficiency and driveability in different driving conditions such as launching (high-torque low-speed) and highway cruising (low-torque high-speed).

Previous research has addressed supervisory control of engine and MG operations as well as mode-shifting strategies to improve fuel efficiency and driveability for a given architecture [1–3]. The attendant question is whether some architectures are more advantageous for some types of vehicles. For example, one might question whether architectures developed for passenger cars and light trucks are suitable for heavy trucks, delivery vans or military vehicles with different specifications and duty (driving) cycles.

*Address all correspondence to this author.

Previous work explored this question using a heuristic search algorithm to find the near-optimal powertrain architecture for given driving cycle and vehicle specifications [4]. It was shown that the solution can be sensitive to vehicle weight. For example, a significantly different solution was found when we changed the vehicle weight from 1400kg to 1600kg. Motivated by this observation, this paper investigates the optimal powertrain architecture design under a distribution of vehicle weights (or payloads).

The paper offers two contributions: (1) We show that an architecture designed to accommodate a variety of vehicle weights (payloads) has better averaged fuel economy than architectures designed for specific weights (payloads); (2) we propose a measure of architecture complexity and use it to reduce the number of feasible mode combinations. In addition, we introduce the final drive ratio as a design variable to be optimized, alongside the optimization of the architecture. This is because the final drive ratio can have a significant impact on vehicle fuel economy and driveablility. We demonstrate in a case study that tractable search of the near-optimal architecture and final drive ratio can be achieved, by limiting the complexity of architectures and incorporating an efficient supervisory control algorithm.

The paper is structured as follows: In Section 2 we review existing work on powertrain architecture design and our previous approach using bond graph representation. Basic familiarity with bond graph terminology is assumed. Section 3 briefly reviews the algorithm to generate driving modes automatically. Section 4 describes the vehicle simulation model. Section 5 discusses the optimal design problem and search process. Section 6 describes application to a case study and the obtained results. We conclude and discuss future directions in Section 7.

2 Previous Work and Backgrounds

Previous research has explored some aspects of hybrid powertrain architecture design. For two-planetary gear power-split architectures, Liu and Peng proposed to generate state-space matrices of driving modes by enumerating feasible combinations of matrix elements [5]. The work assumed that multiple power sources are not connected to the same PG node. Zhang et al. improved the fuel economy of the Prius architecture by adding clutches along connections from the engine, the MGs and the ground to PG nodes, introducing driving modes that disengage the power sources and providing higher torques when the ground is engaged [6]. Zhang et al. also incorporated optimal sizing in architecture design, and achieved tractable computation by adopting a heuristic power management strategy [7].

In the current work, we seek a near-optimal dual-mode architecture[1] by searching heuristically through the entire set of hybrid and pure electric driving modes that consist of one engine, two MGs, two PGs and one ground. In order to do so, we use bond graphs [8] to model power flow in driving modes, an approach common in powertrain analysis and control [2, 9]. Different feasible driving modes can then be created by manipulating bond graph nodes and edges.

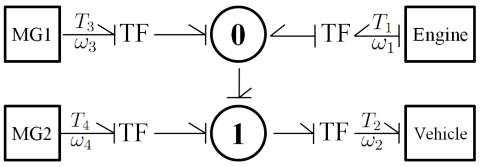

FIGURE 2. The bond graph of the Prius System.

Below we explain briefly the modeling of driving modes using bond graphs. In Figure 1, the engine, the vehicle and the two MGs of the Toyota Prius powertrain are connected via a PG represented by a lever. On the lever, node "R" stands for the ring, "C" for the carrier and "S" for the sun gear. Throughout this paper, we denote the speeds (rads/s) and torques (Nm) coming out from the PG to the engine, the vehicle, MG 1 and MG 2 by $\omega_{1,2,3,4}$ and $T_{1,2,3,4}$, respectively. Assuming that engine and motor inertias are negligible compared with those of the vehicle, the powertrain system can be considered quasi-static. Therefore $\omega_{1,3,4}$ and $T_{1,3,4}$ are equivalent to the engine and motor speeds and torques, while ω_2 and T_2 are the speed and torque demands from the vehicle, rated by the final drive ratio. Given a ring to sun PG ratio ρ, the static torque and speed relationships of the Toyota Prius driving mode are

$$\begin{aligned} (\rho+1)\omega_1 &= \omega_3 + \rho\omega_2, \\ \omega_4 &= \omega_2; \end{aligned} \tag{1}$$

and

$$\begin{aligned} -T_1 &= T_3(1+\rho), \\ T_1\rho + T_4(1+\rho) &= T_2(1+\rho). \end{aligned} \tag{2}$$

The same relationships can also be modeled by the bond graph in Figure 2. In this figure, we use square boxes for external power sources and circles labelled by 0 and 1 for the "0" and "1" junctions. The sign "TF" represents a "transformer" that scales torque and speed simultaneously by a transformer modulus conserving the power at the input and output. For brevity, the transformer blocks will be replaced by bond weights in the rest of the paper.

3 Architecture Generation

In this section we briefly describe how feasible driving modes are generated for given powertrain components. Interested readers are referred to previous work [4] for a more detailed discussion.

[1] We use the term "near-optimal" to acknowledge that the solution found from the proposed heuristic search cannot be proved to be the true optimum, which is the case for most combinatorial optimization problems.

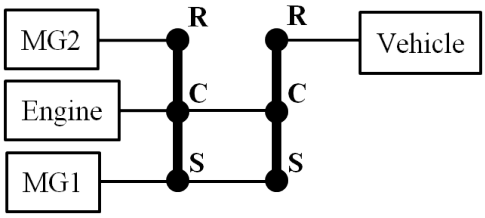

(a) Toyota Prius-like two-PG mode

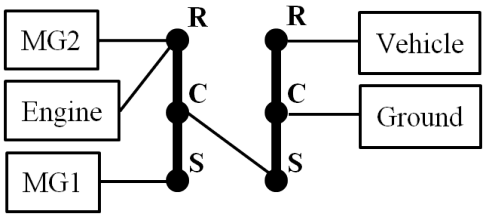

(b) Chevrolet Volt-like two-PG mode, the PG on right serves as an extra final drive.

FIGURE 3. 2-PG modes similar to Toyota Prius in (a) and Chevrolet Volt in (b).

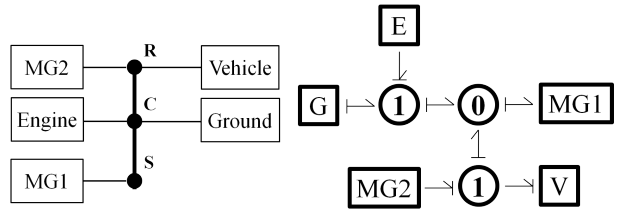

(a) one-PG EV mode, engine engaged to the ground

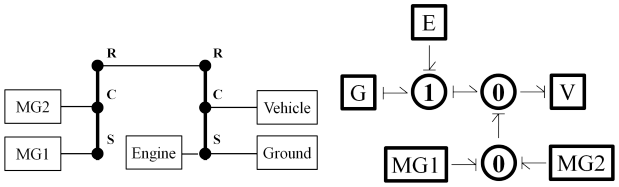

(b) two-PG EV mode, engine engaged to the ground

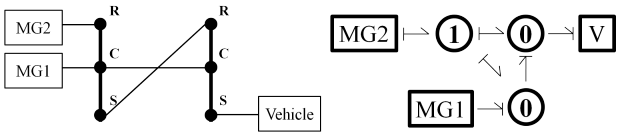

(c) EV mode without engine

FIGURE 4. Examples of EV modes

We group junctions in a bond graph as the "external" junctions, which are dedicated to power sources, and the "internal" junctions, which correspond to "0" and "1" junctions. The four steps for driving mode generation are as follows: (1) Given all power sources and a fixed number of PGs, the number of junctions (nodes) in the bond graph can be determined and all possible undirected graphs can be enumerated; (2) for each undirected graph, binary labels are assigned to internal junctions, and causality strokes are assigned to bonds; (3) bond weights are assigned, determining how the power sources are connected to PG nodes; (4) quasi-static state-space equations can be generated from the bond graphs.

For the powertrain system with one engine, two MGs, two PGs, and the ground, this procedure allowed us to generate a total of 1724 unique driving modes, with 1116 hybrid and 608 electric modes, including patented ones such as those in [2,10,11] as well as the two-PG equivalence of Toyota Prius and the dual-motor mode of Chevrolet Volt. The lever analogy and bond graphs of these driving modes are shown in Figure 3.

Some 559 modes among all discovered ones have the engine grounded (Figures 4(a) and 4(b) for examples) and another 49 have the engine and the ground excluded from the system (Figure 4(c) for example). It should be noted that the current study does not consider multiple grounded PG nodes, nor do we incorporate more complicated PG design such as the Ravigneaux compound PG.

4 Vehicle Modeling

This section describes the modeling details for simulating the fuel consumption for a given driving mode. The mechanical path of the vehicle model consists of a vehicle body connected to the engine and MGs through the PGs as defined by the driving mode. On the electrical path, MGs are connected to the high voltage battery through power electronics.

4.1 Quasi-static powertrain model

In the simulation model we assume that the vehicle follows the drive cycle exactly. Under this assumption and for the given vehicle specifics, the speed and torque requirement to follow the cycle can be calculated as follows. For the torque requirement, T_{req}, we have

$$T_{req} = (F_{acc} + F_{roll} + F_{aero})R_{tire}/FR, \tag{3}$$

where $F_{acc} = M_{veh} \cdot a_{cycle}$ is the force required for the acceleration determined by the vehicle mass M_{veh} and the acceleration at time step t, a_{cycle}. Further, F_{roll}, F_{aero}, R_{tire} and FR are the rolling friction, aerodynamic drag, tire radius and the final drive ratio, respectively.

The speed requirement ω_{req} is calculated as:

$$\omega_{req} = \frac{V_{cycle}}{R_{tire}} \cdot FR, \tag{4}$$

where V_{cycle} is the vehicle speed at time step t.

Considering that the engine control speed profile ω_{eng} and torque T_{eng} for all time steps are given by a supervisory controller, we can calculate the fuel consumption based on the engine model and its consumption map.

In addition, the state-space equations associated with the given driving mode determine the quasi-static relationship between the engine speed and the MG speeds at any given time step:

$$\begin{bmatrix}\omega_{MG1}\\ \omega_{MG2}\end{bmatrix} = C_{mode} \cdot \begin{bmatrix}\omega_{eng}\\ \omega_{req}\end{bmatrix}, \tag{5}$$

where C_{mode} are the kinematic relationship matrices created using the process described in Section 3 for all feasible driving modes. Assuming no energy loss at the PGs, the following power equality holds:

$$P_{eng} + P_{MG1} + P_{MG2} = P_{req}, \tag{6}$$

which leads to the relationship between the engine torque, the torque demand and those at the MGs:

$$\begin{bmatrix}T_{MG1}\\ T_{MG2}\end{bmatrix} = -C_{mode}^{-T} \cdot \begin{bmatrix}T_{eng}\\ -T_{req}\end{bmatrix}. \tag{7}$$

4.2 Battery model

We assume that the DC voltage level is constant and equal to the battery output voltage V_{batt}. We also assume that two MGs are identical, hence they have the same efficiency maps as functions of MG speeds and torques. Given the speed and torque demands for two MGs from Equations (5) and (7), the MG currents are calculated using:

$$I_{mot} = \frac{T_{mot} \cdot \omega_{mot}}{\eta_{mot} \cdot V_{batt}}, \tag{8}$$

and

$$I_{gen} = \frac{T_{gen} \cdot \omega_{gen}}{V_{batt}} \cdot \eta_{gen}, \tag{9}$$

where I_{mot} (T_{mot}, ω_{mot}, η_{mot}) and I_{gen} (T_{gen}, ω_{gen}, η_{gen}) are the currents (torque, speed and efficiency) of the motor and generator, respectively, and V_{batt} is the battery voltage. Note that since each MG can work as both motor or generator, MG currents, I_{MG1} and I_{MG2}, are calculated either from Equation (8) or Equation (9) depending on the type of operation. From these currents, the battery current is calculated as:

$$I_{batt} = \frac{I_{MG1} + I_{MG2}}{\eta_{batt} \cdot \eta_{inv}}, \tag{10}$$

where η_{batt} and η_{inv} are the fixed battery and inverter efficiencies, respectively. The battery state of charge (SOC) is obtained by integrating the following equation over the time horizon,

$$\dot{SOC} = -I_{batt}/C_{batt}, \tag{11}$$

where C_{batt} is the nominal battery capacity.

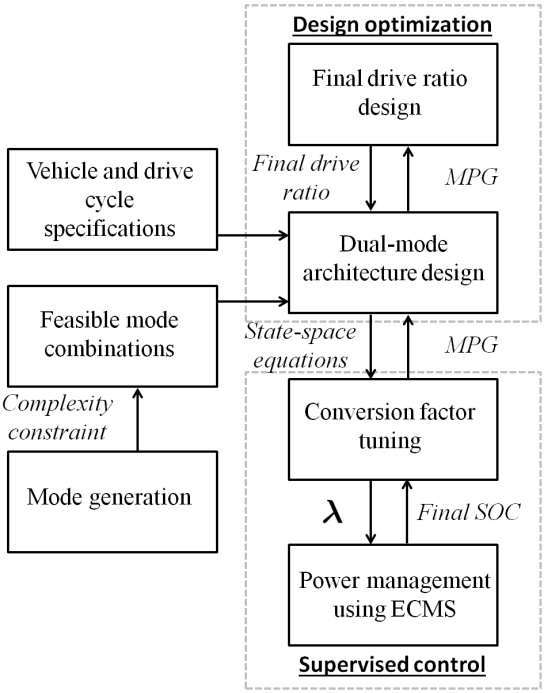

FIGURE 5. The optimal architecture design flow

5 Optimal Architecture Design

We now discuss the search for a dual-mode architecture, i.e., two-mode combination, that achieves near-optimal fuel economy under a distribution of vehicle loads. For given modes, vehicle specifications and drive cycle, the fuel economy of an architecture is evaluated based on the optimal control of the powertrain. We will describe the control strategy first and then introduce the design process. The methods developed in this paper are extensions from our previous work [4], with the following improvements: (1) In addition to the architecture design, an optimal final drive ratio from a discrete set is selected ; (2) to avoid overcomplicated architectures, we filter out those that require more than 4 clutches to accomplish mode-shifting; (3) we simplify the control algorithm to account for the changes in the vehicle in a computationally efficient way. Figure 5 summarizes the design flow.

5.1 Design under a given distribution of loads

Most existing literature on powertrain architecture design assumes a fixed vehicle weight. However, the weight of the vehicle can change from time to time depending on the number of passengers and the weight of payloads. An architecture optimized for a specific weight would work sub-optimally when the vehicle weight changes. Therefore in this paper we propose to optimize the fuel consumption of an architecture averaged over a given distribution of vehicle weights.

5.2 Supervisory control for power management

We develop a supervisory controller to find the near-optimal torque and speed profiles of the engine and MGs that minimize the fuel consumption while meeting the torque and speed demands from the drive cycle. The total fuel consumption can be calculated as:

$$J = \int_0^T \dot{m}_f \cdot dt, \tag{12}$$

where $\dot{m}_f$ is the fuel mass flow rate as a function of engine torque and speed and T is the final time. As opposed to plug-in hybrid vehicle designs, we consider the charge-sustaining constraint which requires the final battery SOC to be the same as the initial SOC, in order to keep the vehicle operating without recharging. The constraints of the optimal control problem can be summarized as:

$$\begin{aligned} SOC(t_f) &= SOC(t_0) \\ SOC_{min} &\leq SOC(t) \leq SOC_{max} \end{aligned}. \tag{13}$$

Based on the drive cycle, i.e., the discrete speed profile for a finite time horizon, and the vehicle specifications, the optimal fuel consumption needs to be derived by controlling the engine and motors in an efficient way and shifting driving modes when appropriate. Various supervisory control strategies have been reported, including load leveling [12, 13], dynamic programming (DP) [14, 15], Equivalent Consumption Minimization Strategy (ECMS) [16–18], and Pontryagin's minimum principle (PMP) [19–21]. While not theoretically optimal, we adopt ECMS for supervisory control for the following reasons: (1) The computational cost for evaluating each architecture is a major consideration since the optimization routine will evaluate a large number of architectures before it converges. While DP can yield the optimal control policy with a fine discretization of time, it is computationally more expensive than ECMS and PMP, which can find solutions close to the optimal one in real time; (2) under the assumptions that (i) battery state of charge (SOC) and battery power are linearly related and (ii) variation in the voltage and the resistance of the battery are negligible within the range of SOC from 40% to 80%, the solutions from ECMS and PMP are equivalent [3]. According to our presented model, both assumptions will hold in this study.

The ECMS algorithm we implemented follows Ahn et al. [22] and more details were documented in [4]. The algorithm introduces an equivalent fuel consumption, denoted by EFC, as follows:

$$EFC = \int_0^T \left(\dot{m}_f + \lambda \cdot \dot{E}_{batt}\right) \cdot dt. \tag{14}$$

Here E_{batt} is the energy currently stored in the battery, and λ is a conversion factor. While λ is time dependent according to PMP, it can be approximated as a constant for the given SOC range.

At each time step, the algorithm chooses the engine speed and torque that minimizes the instantaneous equivalent fuel consumption $\dot{m}_f + \lambda \cdot \dot{E}_{batt}$. For this purpose, some offline calculations are performed: Given the speed and torque demand from the vehicle at each time step, all possible engine operating points and the corresponding MG operating points that satisfy the demand are mapped to the two-dimensional space spanned by the fuel and battery power consumptions. The Pareto-optimal engine-battery consumption points can then be identified. For a given conversion factor λ, the equivalent fuel consumption can be directly minimized by looking up the Pareto curves at all time steps. The correct value of λ should satisfy the charge-sustaining constraint given in Equation (13) and can be found through iterative methods, e.g., the secant method.

The calculation of the aforementioned Pareto curves must be performed for all driving modes, vehicle weights and for all time steps in a drive cycle, and is computationally expensive. To alleviate the computation burden, we investigate how a Pareto curve changes with increasing vehicle weight. Figure 6 compares the Pareto curves at two vehicle weights at the same time step during the drive cycle.

Theoretically, the engine operating points corresponding to one Pareto curve will not necessarily be Pareto optimal when the weight changes. Nonetheless, as shown in Figure 7, our experiments indicate that the engine operating points practically overlap the optimal ones while the vehicle weight changes from 2400 kg to 3400 kg. Figure 8 shows the growth of the error as a function of the vehicle mass where the largest error value corresponds to Figure 7. In other words, while the movement of the Pareto curve in the vertical direction (battery power axis) is significant, the movement in the horizontal direction (fuel consumption axis) is negligible. In fact, under the Urban Dynamometer Driving Schedule (UDDS), applying the optimal engine operating points for a vehicle at 2400 kg to the same vehicle at 3400 kg, but calculating battery power based on the demand from the drive cycle results in a fuel consumption less than 1% different from the optimal. Based on these observations, we calculate the Pareto curves and corresponding engine operating points for the lowest vehicle load and use the same operating points for all other loads. Note that when the final drive ratio changes, the set of Pareto points must be recalculated.

5.3 Complexity constraint

Shifting among driving modes in an architecture is realized through engaging and disengaging clutches. While it is theoretically possible to shift from one mode to another using clutches, the number of clutches should be limited so that the powertrain design can be realized in practice - An architecture with less complexity is preferred as it has lower manufacturing cost, less clutch losses and possibly faster shifting. Below we explain how the number of clutches is calculated for a given pair of driving modes.

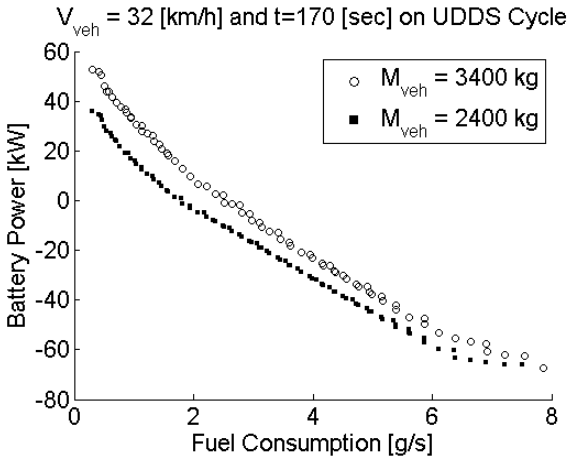

FIGURE 6. Comparison of the optimal operating points for two different vehicle loads

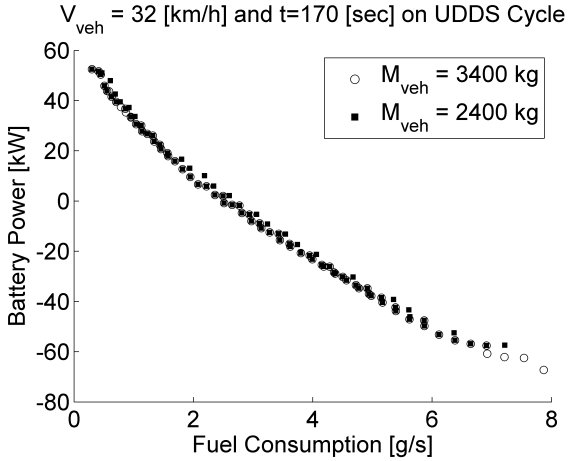

FIGURE 7. Overlap between optimal engine operating points for two different vehicle masses

To start, we introduce a binary connectivity table. The table has eleven rows and six columns for a two-PG system. The first five rows correspond to the engine, the vehicle output, MG1, MG2 and the ground, respectively. The remaining six rows, and the six columns, correspond to the sun, ring and carrier gears of each PG, respectively. Given a bond graph representing a driving mode, a table entry will have "1" when the corresponding two components are connected.

As demonstrated in Figures 9 and 10, the number of clutches needed for a dual-mode architecture can be calculated by comparing the two associated connectivity tables. Note that in this study the two MGs have the same specs and the PGs have the same ratio. Therefore multiple clutching solutions are possible for a given pair of driving modes (Figure 9). In such cases, we use the minimum number of clutches as a complexity measure

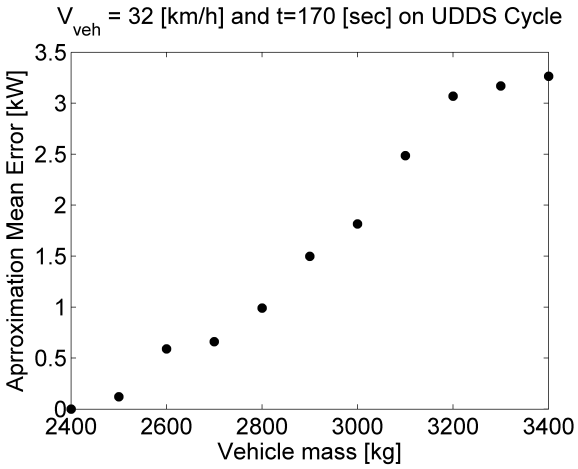

FIGURE 8. Growth of the mean error in the control approximation as function of vehicle mass

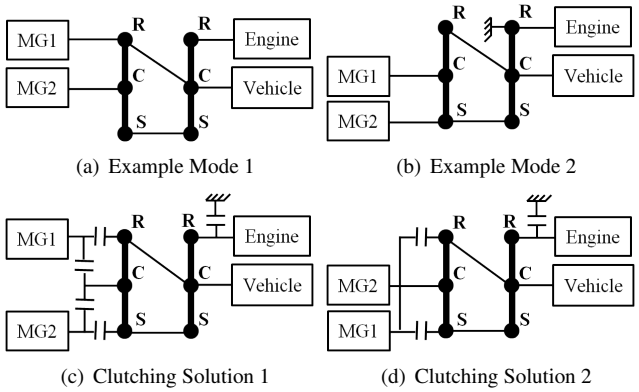

(a) Example Mode 1 (b) Example Mode 2

(c) Clutching Solution 1 (d) Clutching Solution 2

FIGURE 9. Multiple clutching solutions obtained by changing MG definitions

(Figure 10). In addition, solutions that require a clutch at the vehicle output shaft are considered infeasible since it is not desired to disconnect the vehicle output from the power sources.

5.4 Search method

The same unidirectional search algorithm as proposed in [4] are used: We start with an initial mode and enumerate all modes to find the other one so that the pair has the minimum fuel consumption; then we fix the newly-found mode and enumerate again to replace the initial mode. The search terminates when no better combination can be found. Note that the solution can be sub-optimal as the search is not exhaustive.

6 Case Study and Results

In this section, we present a case study and discuss the results.

	S1	C1	R1	S2	C2	R2
Engine	0	0	0	0	0	1
Vehicle	0	0	1	0	1	0
MG1	0	0	1	0	1	0
MG2	0	1	0	0	0	0
Ground	0	0	0	0	0	0
S1	0	0	0	1	0	0
C1	0	0	0	0	0	0
R1	0	0	0	0	1	0
S2	1	0	0	0	0	0
C2	0	0	1	0	0	0
R2	0	0	0	0	0	0

Example Mode 1

2 clutches

1 clutch

	S1	C1	R1	S2	C2	R2
Engine	0	0	0	0	0	1
Vehicle	0	0	1	0	1	0
MG1	0	1	0	0	0	0
MG2	1	0	0	1	0	0
Ground	0	0	0	0	0	1
S1	0	0	0	1	0	0
C1	0	0	0	0	0	0
R1	0	0	0	0	1	0
S2	1	0	0	0	0	0
C2	0	0	1	0	0	0
R2	0	0	0	0	0	0

Example Mode 2

FIGURE 10. Connectivity tables for the example modes in Figure 9. The minimum number of clutches required is 3, when the two MGs are identical.

6.1 Model specification

Table 1 lists specifications of the vehicle used in this case study. The engine and motors are represented by their corresponding consumption and efficiency maps, with speed and torque limits specified. Battery efficiency is fixed at 92% and power electronics efficiency at 95%. The state-space matrices for all driving modes are calculated offline and all Pareto curves derived. The engine and motor operating points, as well as the mode-shifting strategy, are then determined by the supervisory controller described in Section 5.2. As part of the control strategy, the initial battery state of charge is set at 60% and is sustained at the end of the simulations. In order to prevent frequent mode shifts, we assign a fixed penalty of 0.1 grams equivalent fuel consumption to each shift. A parametric study on this penalty should be investigated in future work. The UDDS cycle is used.

6.2 Simulation results and discussion

Two scenarios are considered and compared for fuel economy optimization: (1) The vehicle with baseline weight (2400 kg) and (2) the same vehicle under a distribution of weights. In the latter case, the vehicle weight is varied from 2400 to 3400kg in five equal steps. We assume each loading condition to be equally probable.

The optimal dual-mode architectures for the two scenarios are shown in Figures 11 and 12 and referred to as design A and design B, respectively. Design A results in a fuel economy of 40.72 miles per gallon (MPG) in the first scenario, and design B has an averaged fuel economy of 37.42 MPG over all assumed weights. When tested using the distribution of weights, design A results in an averaged fuel economy of 36.51 MPG, inferior to design B. In addition, the significant difference between the two architectures can be observed from the figures. These results show the necessity for considering the distribution of vehicle weights (or loads) during the design process in order to identify the correct fuel efficient architecture.

Specification	Value
Mass (weight)	2400 - 3400 [kg]
Tyre radius	0.4 [m]
Frontal area	3.2 [m^2]
Aerodynamic drag coefficient	0.45
Final drive ratios	2 - 6
Ring to Sun gear ratio	2
Battery voltage	350 [V]
Battery nominal capacity	13.8 [Ah]
Electric motor output power	75 [kW]
Engine displacement size	6.5 [L]
Engine output power	140 [kW]

TABLE 1. Vehicle Specifications

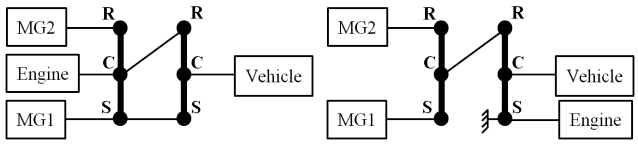

(a) Hybrid mode

(b) Pure electric mode

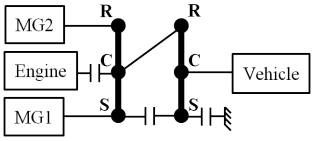

(c) Architecture

FIGURE 11. Optimal solution for the baseline case, with an optimal final drive ratio of 5

The approximation we make for the control policy in Section 5.2 does not affect those results significantly. For instance the averaged fuel economy of the design B without the approximation is 37.46 MPG which is marginally larger than the approximated value.

To understand the effect of the final drive ratio, we use Figure 13 to show the impact of the final drive ratio on the fuel economy for the design in Figure 12. The significant change in MPG indicates the importance of including the final drive ratio as a variable in optimization.

Following the progress of the optimization process towards termination, some sub-optimal yet less complex designs were generated, such as the one shown in Figure 14. This design has

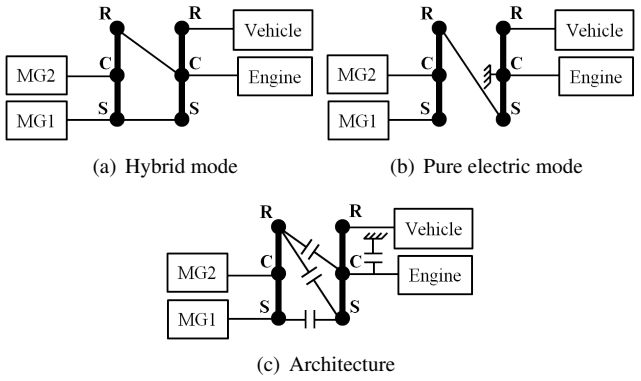

FIGURE 12. Optimal solution for the vehicle under the distribution of weights, with an optimal final drive ratio of 5.5

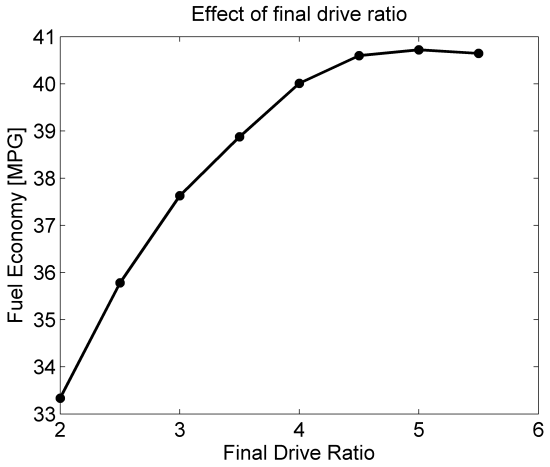

FIGURE 13. Impact of the final drive ratio on the fuel economy for the design in Figure 11.

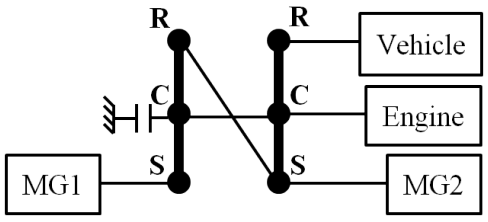

FIGURE 14. A simple architecture only marginally worse than the optimal one.

an averaged fuel economy of 36.90 MPG over the distribution of weights, which is only marginally less efficient than the optimal design in Figure 12. Such a design could be preferred over the optimal one if cost and manufacturing considerations are taken into account.

7 Conclusion

Motivated from earlier studies indicating that an optimal EV powertrain architecture could be sensitive to small changes in vehicle weight, we presented a new study to determine an overall best architecture given scenarios of varying loadings.

Since such a search with a nested control problem is computationally expensive, a novel heuristic approach was introduced to reduce the computational cost of vehicle control, along with an architecture complexity constraint that tightens the search space. The final drive ratio was also included as a design variable and shown to have significant impact.

The results from the case study showed that a near-optimal powertrain architecture designed for a specific weight will have inferior fuel economy under a distribution of weights (loads). Therefore, incorporating the distribution of loading conditions into the architecture design problem is necessary. The impact of different weight distributions on the near-optimal results should be investigated. Also this conclusion should be further validated by performing a parametric study on a broader range of vehicle weights and a variety of drive cycles.

Further investigation should address a better search algorithm of the architecture by improving its heuristics with knowledge learned from the searched architectures. In addition, the computational cost of the nested optimal control problem would need to be further reduced to enable introduction of additional design variables such as PG ratio and motor/engine sizing.

Acknowledgement

This research was partially supported by the Automotive Research Center, a US Army Center of Excellence in Modeling and simulation of Ground Vehicle Systems headquartered at the University of Michigan, and by the University of Michigan - General Motors Collaborative Research Laboratory in Advanced Powertrains. This support is gratefully acknowledged. The authors would also like to thank Professor Huei Peng and Xiaowu Zhang from the University of Michigan for their insightful advice. The opinions expressed here are solely those of the authors.

REFERENCES

[1] Liu, J., Peng, H., and Filipi, Z., 2005. "Modeling and control analysis of toyota hybrid system". In IEEE/ASME International Conference on Advanced Intelligent Mechatronics. Proceedings,, IEEE, pp. 134–139.

[2] Kim, N., Kim, J., and Kim, H., 2008. "Control strategy for a dual-mode electromechanical, infinitely variable transmission for hybrid electric vehicles". *Proceedings of the Institution of Mechanical Engineers, Part D: Journal of Automobile Engineering,* ***222***(9), pp. 1587–1601.

[3] Serrao, L., Onori, S., and Rizzoni, G., 2009. "Ecms as a realization of pontryagin's minimum principle for hev con-

trol". In American Control Conference, IEEE, pp. 3964–3969.

[4] Bayrak, A. E., Ren, Y., and Papalambros, P. Y., 2013. "Design of hybrid-electric vehicle architecture using auto-generation of feasible driving modes". In Proceedings of the ASME 2013 International Design Engineering Technical Conferences, ASME.

[5] Liu, J., and Peng, H., 2010. "A systematic design approach for two planetary gear split hybrid vehicles". *Vehicle System Dynamics,* ***48***(11), pp. 1395–1412.

[6] Zhang, X., Li, C.-T., Kum, D., and Peng, H., 2012. "Prius+ and volt- : Configuration analysis of power-split hybrid vehicles with a single planetary gear". *IEEE Transactions on Vehicular Technology,* ***61***(8), pp. 3544–3552.

[7] Zhang, X., Peng, H., and Sun, J., 2013. "A near-optimal power management strategy for rapid component sizing of power split hybrid vehicles with multiple operating modes". In American Control Conference (ACC), 2013, pp. 5972–5977.

[8] Karnopp, D. C., Margolis, D. L., and Rosenberg, R. C., 2012. *System Dynamics: Modeling, Simulation, and Control of Mechatronic Systems*, 5th ed. Wiley, Hoboken, NJ.

[9] Chan, C.-C., Bouscayrol, A., and Chen, K., 2010. "Electric, hybrid, and fuel-cell vehicles: Architectures and modeling". *Vehicular Technology, IEEE Transactions on,* ***59***(2), pp. 589–598.

[10] Ai, X., and Anderson, S., 2005. "An electro-mechanical infinitely variable transmisson for hybrid electric vehicles". *SAE Technical Paper 2005-01-0281, doi:10.4271/2005-01-0281*.

[11] Schmidt, M., 1999. Electro-mechanical powertrain, Aug. 10. US Patent 5,935,035.

[12] Hermance, D., 1999. "Toyota hybrid system". In 1999 SAE TOPTEC Conference, Albany, NY.

[13] Jalil, N., Kheir, N. A., and Salman, M., 1997. "A rule-based energy management strategy for a series hybrid vehicle". In American Control Conference, 1997. Proceedings of the 1997, Vol. 1, IEEE, pp. 689–693.

[14] Lin, C.-C., Peng, H., Grizzle, J. W., and Kang, J.-M., 2003. "Power management strategy for a parallel hybrid electric truck". *Control Systems Technology, IEEE Transactions on,* ***11***(6), pp. 839–849.

[15] Liu, J., and Peng, H., 2006. "Control optimization for a power-split hybrid vehicle". In American Control Conference, 2006, IEEE, pp. 6–pp.

[16] Paganelli, G., Delprat, S., Guerra, T.-M., Rimaux, J., and Santin, J.-J., 2002. "Equivalent consumption minimization strategy for parallel hybrid powertrains". In Vehicular Technology Conference, 2002. VTC Spring 2002. IEEE 55th, Vol. 4, IEEE, pp. 2076–2081.

[17] Sciarretta, A., Back, M., and Guzzella, L., 2004. "Optimal control of parallel hybrid electric vehicles". *Control Systems Technology, IEEE Transactions on,* ***12***(3), pp. 352–363.

[18] Stockar, S., Marano, V., Rizzoni, G., and Guzzella, L., 2010. "Optimal control for plug-in hybrid electric vehicle applications". In American Control Conference (ACC), 2010, IEEE, pp. 5024–5030.

[19] Delprat, S., Lauber, J., Guerra, T. M., and Rimaux, J., 2004. "Control of a parallel hybrid powertrain: optimal control". *Vehicular Technology, IEEE Transactions on,* ***53***(3), pp. 872–881.

[20] Delprat, S., Guerra, T., and Rimaux, J., 2002. "Control strategies for hybrid vehicles: optimal control". In Vehicular Technology Conference, 2002. Proceedings. VTC 2002-Fall. 2002 IEEE 56th, Vol. 3, IEEE, pp. 1681–1685.

[21] Kim, N., Cha, S., and Peng, H., 2011. "Optimal control of hybrid electric vehicles based on pontryagin's minimum principle". *Control Systems Technology, IEEE Transactions on,* ***19***(5), pp. 1279–1287.

[22] Ahn, K., Cho, S., and Cha, S., 2008. "Optimal operation of the power-split hybrid electric vehicle powertrain". *Proceedings of the Institution of Mechanical Engineers, Part D: Journal of Automobile Engineering,* ***222***(5), pp. 789–800.